Acta Materialia 236 (2022) 118105

Contents lists available at ScienceDirect

Acta Materialia

journal homepage: www.elsevier.com/locate/actamat

Full length article

Critical assessment of the extreme mechanical behavior of a stable nanocrystalline alloy under shock loading

B.C. Hornbuckle[a,*], S.A. Turnage[a], C.L. Williams[a], A.K. Giri[a], D. Casem[a], K. Solanki[b], K.A. Darling[a]

[a] DEVCOM Army Research Laboratory, Weapons and Materials Research Directorate, APG, MD 21005, USA
[b] School for Engineering of Matter, Transport, and Energy, Arizona State University, Tempe, AZ 85287, USA

ARTICLE INFO

Article history:
Received 22 March 2022
Revised 3 June 2022
Accepted 16 June 2022
Available online 17 June 2022

Keywords:
Nanocrystalline alloys
Cu-Ta
TEM
Interfaces and defects

ABSTRACT

A material's spall-strength and Hugoniot elastic limit (HEL), are measures of its ability to resist failure and plastic deformation under shock loading. An ideal single-crystal, i.e., a defect-free material, offers perfect lattice rectification, and therefore, provides an upper bound, or expected limit, which has yet to be exceeded by their polycrystalline counterparts. Toward this, we used a nanocrystalline (NC) copper-tantalum alloy, a model system, to probe the HEL and the spall strength of a stable NC alloy and the pertaining microstructural features that control failure. The results reveal significant increases in the HEL to about 2.0 GPa and spall strength of 1.19–1.67 GPa compared to polycrystalline Cu along with negligible changes in the residual hardness and microstructure of the shock recovered samples. The observed spall strength is approximately 2-times that of polycrystalline Cu. Further, advanced microstructural characterization using transmission electron microscopy (TEM) found no increase in dislocation density and/or mechanical twinning between the as-received and shock recovered samples, i.e., stabilized NC-alloys exhibit an unprecedented ability to resist high defect (such as dislocation) accumulation and damage. This anomalous behavior in stable NC-alloys is attributed to the elimination/limitation of defects formed under shock conditions coupled with a divergent strain-rate-insensitive behavior of its main microstructural features. The present work highlights, if designed properly, that some critical lower length-scale features including grain and phase boundaries may not contribute to the failure process. However, more fundamental research is needed to address the role processing parameters have on the resultant material that could result in spall strengths comparable to those attained for single crystals.

Published by Elsevier Ltd on behalf of Acta Materialia Inc.

1. Introduction

The damage tolerance of metals under shock loading is strongly related to the type and concentration of defects present in the material. Under the extreme conditions of shock loading, defects are localized regions of disruption to the perfect crystalline order and therefore represent weak points within the landscape of its atomic periodicity. Shock wave propagation through a solid necessitates that the entire volume, containing defects, will experience a compressive load. During the compressive phase of shock loading, the existing defects become proliferated with the nucleation and accumulation of the newly created defects. This non-equilibrium concentration of defects evolves into damage and consequent failure of the material. Spall failure or spallation occurs as a result of rarefaction waves interacting within this volume of defects to produce high tensile stresses to cause cavitation (i.e. the nucleation and coalescence of voids) at its weakest points [1]. A material's response to this process can be quantified through its Hugoniot elastic limit (HEL) and spall strength, which are measures of its ability to resist plastic deformation and failure under shock loading. An ideal single crystal, i.e., a defect-free material, offers perfect lattice rectification, and therefore, provides an upper bound, or expected limit, for a material's spall strength which has yet to be exceeded by its alloyed counterpart [2]. This behavior has been routinely confirmed for all structures of metals through experimental shock studies using single-crystal samples, which show a factor of 2–4 times higher spall strength than that of their conventional counterparts that contain defects [3,4]. Therefore, the ability to absorb and/or mitigate/arrest the presence/generation of defects (weak points) will inherently increase spall strength in metals.

On the contrary, and for the past hundred years, the progression of structural engineering metals and alloys has been predicated upon introducing extremely high concentrations of grain

* Corresponding author.
E-mail address: billy.c.hornbuckle.civ@army.mil (B.C. Hornbuckle).

https://doi.org/10.1016/j.actamat.2022.118105
1359-6454/Published by Elsevier Ltd on behalf of Acta Materialia Inc.

boundaries, phase boundaries, stacking faults, and dislocation cell structures to provide sources of strengthening [5–7]. At the most extreme end of this, are bulk nanocrystalline/structured metals that exhibit extreme strengths and altered physical responses attributed to having engineered internal defect concentrations such as grain boundaries and phase boundaries that comprise over 50% of their internal volume. However, this design strategy goes against the logic of ideal single crystal behavior with respect to designing materials to resist failure during high-velocity impact and shock loading events. Specifically, with respect to grain size, many experimental and modeling studies have shown perplexing behavior with higher concentrations of defects (Hall Petch effects) on a material's spall strength [4,8–12]. For instance, Chen et al. [9] and Escobedo et al. [11] found no effects of grain size on spall strength for copper. While Minich et al. [4] found that the high purity single crystals exhibit the highest spall strength followed by the large, medium, and small grain size polycrystalline samples (anti-Hall-Petch effect). In addition, Remington et al. [12] found a significant effect of grain size on the spall strength in tantalum, which is opposite to the prediction of the Hall-Petch relationship. Also intuitively, decreasing grain size increases the number of potential void nucleation sites and hence, the spall strength should be expected to drop. Furthermore, spallation is a complex process strongly influenced by the shock wave profile and microstructure of the sample before the material undergoes tension. The influence of the individual characteristics of the shock wave profile such as shock rise time, pulse duration, peak shock stress, release rate, and pre-shocked microstructure on damage evolution is not well understood. Therefore, more controlled shock compression research is required to fully understand the effects of grain size on spall strength.

With respect to NC grain sizes, to date, this paper represents only the second publication ever to report on the experimental shock testing of bulk NC metals (average grain size $\leq$ 100 nm in all three dimensions) and sample size $>$ 5 mm in 3 dimensions. The lack of publications is due to the difficulties in consolidating NC metals because of their poor thermal microstructural stability as well as overall sample dimensions. Consequently, the vast majority of the literature has been devoted to computational modeling efforts of simulated microstructures, especially atomistic modeling which are inherently affected by time and length scale issues [13–17]. With regard to the limited experimental studies, the work has utilized laser-driven compression of physically deposited thin films or electrodeposits. However, the physics governing wave propagation and its ability to obtain an equilibrium state in laser-based experiments leaves many questions as to the stress state within the material. An active debate on comparing and drawing definitive conclusions between laser-driven experiments to conventional shock recovery studies is still ongoing [18,19].

In addition to grain boundaries, inclusions and secondary-phase particles are known to be potential heterogeneous nucleation sites for micro-voids and crack initiation [2]. Numerous studies exist in which the fracture surface and cross-sections revealed that micron and submicron-sized precipitates were responsible for the initiation of spall failure of the samples [2]. This occurs for three main reasons: (1) changes in density across the matrix-precipitate interface give rise to impedance mismatches and the formation of potential void nucleation sites via matrix-precipitate debonding or precipitate cracking during compression. (2) Larger particles as found in conventional alloys, i.e., particles $>$ 100 nm will tend to have incoherent interfaces with the matrix that are mechanically weaker than fully coherent ones. (3) Reinforcing/strengthening secondary phases tend to be harder, typical examples include stoichiometric compounds, e.g ceramics, and intermetallics phases. Such compounds are brittle compared to the surrounding host matrix and tend to fragment or cleave via unstable crack propagation. Thus, the capability to optimize resistance to spall failure relies on the ability to engineer the interface configuration, morphology, and length-scale of secondary phases under shock loading. Overall, all the above studies indicate that microstructure plays a significant role in spall failure, and the spall strength is largely affected by the presence of interfaces be it grain or phase boundaries. The question remains, given the overwhelming data that suggests interfaces (grain and phase boundaries) are detrimental to the spall performance of a material, is it then possible to then stabilize these defects such that polycrystalline or nanocrystalline metals can exhibit single crystal like spall strength. If possible, then engineering such stability would result in an anomalous deformation behavior relative to what is currently understood through the available modeling and limited experimental efforts on the shock behavior of NC metals.

In the present work, we identify that in a microstructurally stable NC metal, if designed properly, some critical lower length-scale features including grain and phase boundaries may not contribute to the failure process thereby enhancing the spall strength. Toward this, in this work, we use NC Cu-Ta as a model system to probe the HEL and the spall strength of a stable NC alloy, and relevant microstructural features that control failure. The results reveal a significant increase in the HEL to about 2.0 GPa and the spall strength of 1.19–1.67 GPa as compared to polycrystalline Cu alloys along with negligible changes in the residual hardness and microstructure of shock recovered samples. We attribute this anomalous behavior in stable NC alloy to the elimination/limitation of defects induced under shock conditions due to the rarefaction process coupled with a divergent strain-rate insensitive behavior of its main microstructural features. In other words, the present work highlights a critical role of the microstructural length scale below which a material's ability to resist defect accumulations and fracture increases, resulting in the enhanced spall strength (some 50-100% increase) over polycrystalline Cu. Note that the spall strength of single-crystal Cu is 4.5 GPa which is 5.6 times higher than the reported spall strength and 90 times higher then the quasi static yield strength coarse polycrystalline Cu [20]. More specifically, 4.5 GPa is $\sim$ 4.5 times higher than the quasi static yield strength of NC Cu-Ta alloys.

2. Experimental

2.1. Powder processing and consolidation via equal channel angular extrusion (ECAE)

NC Cu-3Ta (at.%) powders were processed utilizing high-energy cryogenic mechanical alloying. Elemental Cu and Ta powders ($\sim$325 mesh and 99.9% purity) were loaded into a hardened steel vial in the appropriate proportion along with the milling media (440C stainless steel balls) inside a glove box with an Ar atmosphere (oxygen and H_2O are $<$ 1 ppm). The vials were loaded with 10 g of Cu-Ta powder as well as the appropriate amount of media to ensure a ball-to-powder ratio of 5-to-1 by weight. A SPEX 8000 M shaker mill was utilized to perform the milling at cryogenic temperature (verified to be $\sim$ -196 °C) for 4 h using liquid nitrogen. The NC Cu-3Ta powder was consolidated to bulk via equal channel angular extrusion (ECAE). For the ECAE consolidation process, the as-milled powder was placed into nickel cans and sealed inside the glove box. Before starting the ECAE process, the die assembly used for processing the billets was preheated to 623 K (350 °C) to minimize thermal loss during the ECAE processing. The billets, heated and equilibrated to 973 K (700 °C) for 40 min, were dropped into the ECAE tooling as quickly as possible from the furnace and extruded at a rate of 25.5 mm/s. These steps were repeated 4 times following route B_C to prevent imparting a texture to the consolidated powder. By extruding through an angle of 90°, a total strain

of 460% was imparted onto the powder-containing billet as a result of processing.

2.2. Shock sample preparation and experiments

Shock compression experiments were performed using cylindrical specimens of NC Cu-3Ta (at.%) alloy that was synthesized with the desired NC microstructure using powder processing techniques and controlling parameters such as milling temperature, milling time, and ECAE temperature. The progression of an ECAE processed nickel can to the final machined test specimen is as follows. A core (approximately 12 mm in diameter) containing the consolidated NC-Cu–3Ta powder was machined from the center of the rectangular nickel billet along the long axis using electric discharge machining (EDM). A live center was created at the tip of the NC-Cu–3Ta rod to reduce wobble during turning operations. The remnants of the Ni-can were removed by turning on a Haas ST10 CNC lathe using a Sandvik CNMG 12 04 08-PM 4325 cutting insert with a cutting speed of 84 cms^{-1} (2000 rpm), a feed of 0.08 mm per revolution at a cutting depth of 0.130 mm per pass to reveal the consolidated NC Cu–3Ta rod being 10 mm in diameter. This rod was sectioned into 3 and 6 mm thick cylindrical specimens using wire Electrical Discharge Machining (EDM) for time-resolved *in-situ* and recovery shock experiments.

Spall experiments are carried out using the light gas guns within the Impact Physics Branch of DEVCOM. For time-resolved *in-situ* spall experiments, OFHC Cu flyer plates of 1.5 mm thickness are accelerated to nominal impact velocities of approximately 0.2, 0.3, 0.5, 0.6, and 1.9 km/s, respectively. For spall recovery experiments, OFHC Cu flyer plates of 1.5 mm thickness are accelerated to nominal impact velocities of approximately 0.3 and 0.6 km/s, respectively. The nanocrystalline specimens are small due to limitations in processing, so the specimens were press-fitted into OFHC Cu specimen holders with approximate impedance to achieve the appropriate geometry (30 mm diameter x 3 mm thick and 30 mm diameter x 6 mm thick for time-resolved *in-situ* and recovery shock experiments) required for mitigating rogue edge release waves.

Free surface velocity is measured using heterodyned photon Doppler velocimetry (PDV). Oscilloscopes for capturing the PDV signal are triggered with electrical shorting pins flush with the impact face of the sample, which also measures the tilt between the flyer and the sample. All tilt measurements were found to be within the required 5 mrad.

The pullback velocity is measured from the resulting free surface velocity-time profile extracted from the acquired PDV signal and the spall strength (σ_s) is calculated as described in [21] and listed here

$$\sigma_s = \frac{1}{2}\left(\Delta v_{fs} + \delta\right)\rho_0 c_0 \tag{1}$$

where Δv_{fs}, the pullback velocity, is the difference between the peak free surface velocity and the minimum free surface velocity just prior to the arrival of the spall pulse, ρ_0 is the density of the material prior to shock compression, and c_0 is the bulk sound speed. The δ in Eq. (1) is a correction factor applied to account for elastic-plastic properties of the sample and is determined by

$$\delta = \left(\frac{h_s}{c_l} - \frac{h_s}{c_F}\right)|\dot{u}_1| \tag{2}$$

where h_s is the spalled plate thickness, c_l is the longitudinal elastic wave speed, $\dot{u}_1$ is the gradient of the velocity-time profile just ahead of the spall pulse, and c_F is the spall pulse propagation velocity determined by

$$c_F = c_0 c_l \sqrt{\frac{\dot{\sigma}_{x+} - \dot{\sigma}_{x-}}{c_l^2\dot{\sigma}_{x+} - c_0^2\dot{\sigma}_{x-}}} \tag{3}$$

where $\dot{\sigma}_{x+}$ and $\dot{\sigma}_{x-}$ are approximations of the time derivatives of the stress ahead and behind the spall pulse as determined by

$$\begin{aligned}\dot{\sigma}_{x+} &\approx \rho_0 c_0 \dot{u}_1/2 \\ \dot{\sigma}_{x-} &\approx \rho_0 c_0 \dot{u}_2/2\end{aligned} \tag{4}$$

where $\dot{u}_2$ is the gradient of the velocity-time profile at the spall pulse. Using conservation of linear momentum, the peak shock stresses were estimated to be in the range of 4.3–39.3 GPa.

2.3. Microstructural characterization

Specimens for TEM characterization were prepared one of two ways. Conventional sample preparation was utilized for the as-received condition. For the shock recovered specimen, the site-specific lift-out technique was performed using an FEI Nova600 Nanolab Dual Beam SEM/FIB. For the conventional process, a 3 mm diameter disk from the bulk specimen was thinned to approximately 100 µm. The sample was then dimpled to $\geq$ 10 µm followed by ion milling with a Gatan Precision Ion Polishing System (PIPS) until the specimen is perforated, generating electron-transparent regions for analysis.

The spall recovery samples were cross-sectioned with a diamond wafering saw exposing the thickness of the specimen. Vickers micro-hardness was performed using a Wilson Hardness Tukon 1202 tester to measure the hardness of the sample exposed to peak stress of 10.9 GPa. To do such measurements, the spalled specimens were taken through a grinding and polishing procedure that ended with at least a 1-micron diamond suspension step. The individual indents were generated using a 100 g force and held for 10 s. The hardness measurements were taken through the specimen thickness via a matrix (34 rows by 5 columns) with 75 µm spacing between each indent. The hardness of the 5 column positions was then averaged and error calculated to yield the hardness value at the respective distances reported. The TEM lift-outs were then taken from two regions of interest, first: parallel to the spall surface located approximately 320 microns below, and second: perpendicular to the spalling surface located exactly on the free fracture surface. All (S)TEM images were captured using a JEOL 2100F microscope operated at 200 kV. In addition to this, SEM secondary and backscatter electron images were taken directly from the fracture surface as well as prepared through-thickness cross-sections utilizing a Hitachi 4700 SEM, (optical images were also collected).

3. Results and discussion

As a starting point and baseline for comparison, Fig. 1(A, B) provides the primary microstructural characterization for the as-received NC Cu-3Ta alloy. Primary microstructural analysis of the as-consolidated samples using TEM indicates that the extruded microstructure for this alloy was found to have an average grain size of 100 $\pm$ 15 nm with Ta-based nanoclusters having an average diameter of 3.2 $\pm$ 0.9 nm. Characterizing the nanocluster matrix coherency relationship at room temperature has indicated that this material has coherent, semi-coherent, and incoherent Ta-based nanoclusters (d $<$ 3.9 nm, 3.9 to 15.6 nm, and $>$15.6 nm, respectively). Atom probe tomography has determined that approximately 90% of the clusters exhibit diameters $<$ 4 nm with cluster number densities of approximately 5.4 $\times$ $10^{23}/m^3$. Therefore, the vast majority of nanoclusters exhibit a coherent relationship with the Cu matrix. Additionally, these Ta-based clusters can be found located along grain boundaries and triple junctions. Extensive modeling efforts have been devoted to understanding the interactions between these Ta clusters and these types of boundaries. Both the modeling efforts and experimental results have proven the clusters prevent not only grain boundary sliding and rotation but grain growth as well [22,23]. While the Ta clusters interact

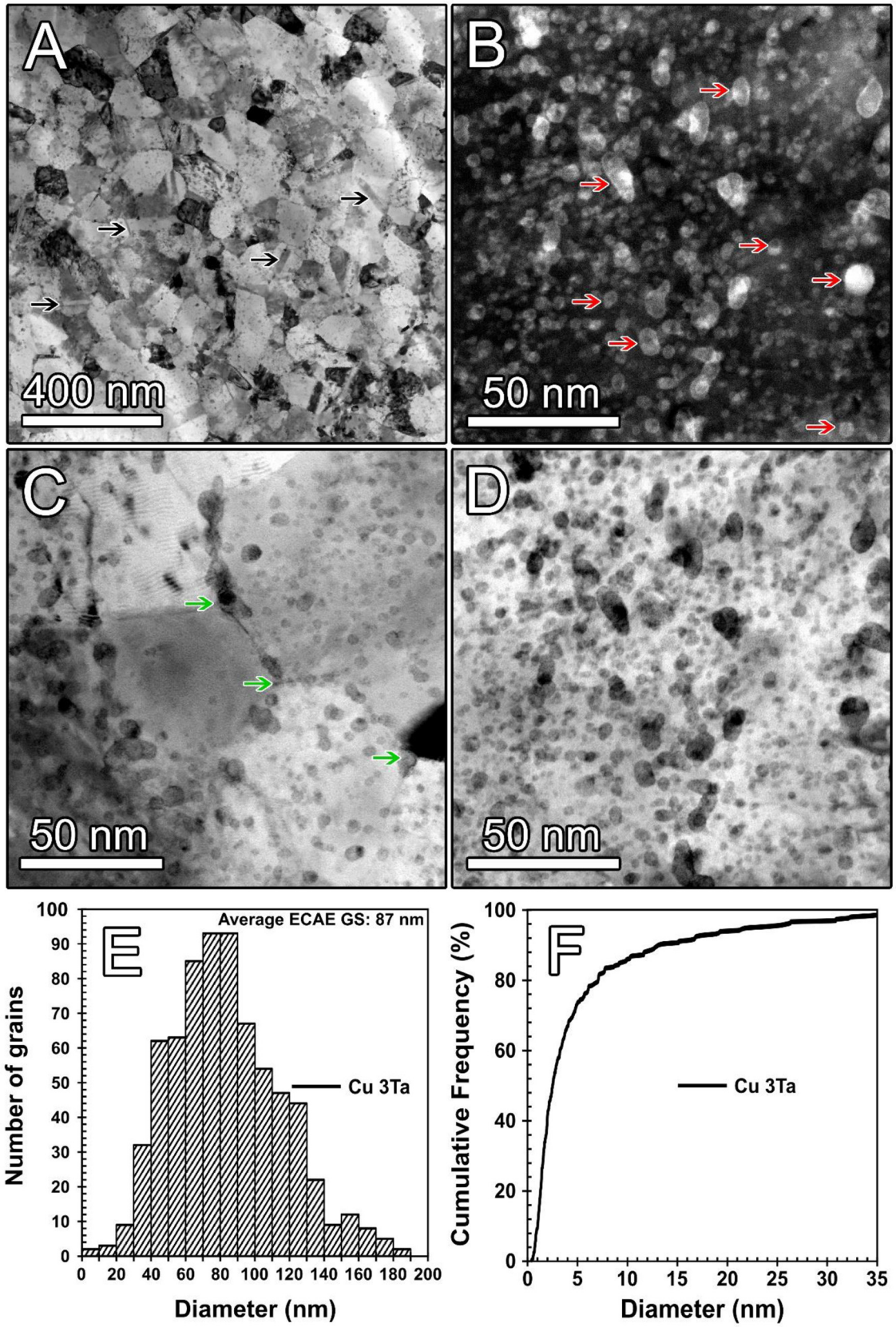

Fig. 1. (A) Low magnification (scanning) transmission electron microscopy (S)TEM Bright Field (BF) image of as-received (i.e., post-ECAE processed) sample showing grain structure (black arrows pointing to twin boundaries). (B) Higher magnification STEM High Angle Annular Dark Field (HAADF) image showing the high density of Ta-based clusters residing in the lattice as well as along the grain boundaries of the Cu-based matrix (red arrows highlighting phase boundaries between Ta-based clusters and Cu matrix). (C) Higher magnification (S)TEM Bright Field (BF) image of as-received sample showing the lack of dislocation structure within grain interiors (green arrows pointing to triple junctions). (D) Corresponding (S)TEM Bright Field (BF) image of (B) highlighting the Ta-based clusters. (E) Grain size histogram for as-received (ECAE-processed) for Cu-3Ta. (F) Cumulative distribution plot of diameter for the Ta-based clusters.

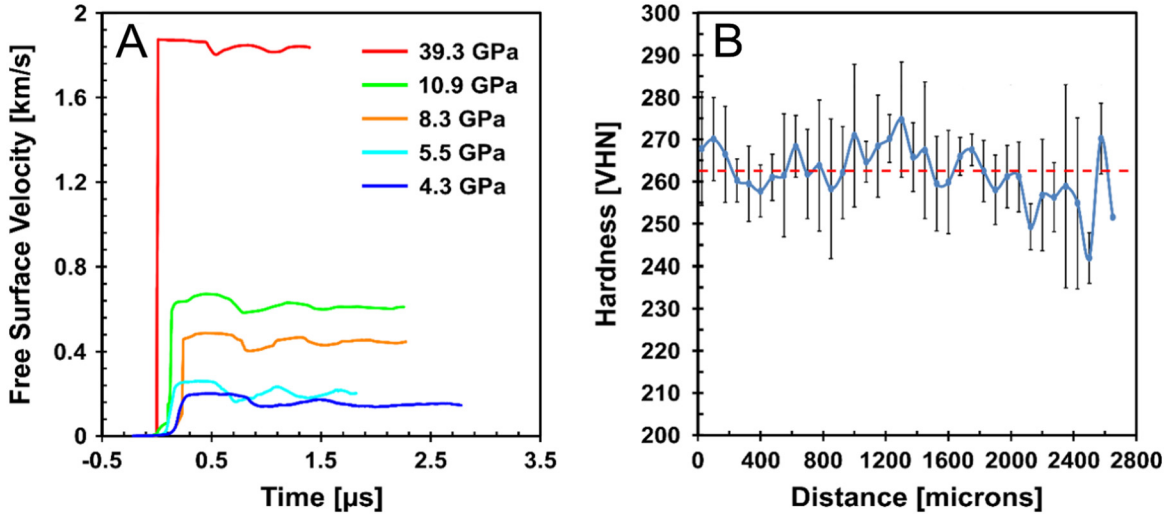

Fig. 2. (A) Time-resolved free surface velocity profiles and (B) The hardness of the as-received NC–Cu–3Ta alloy sample (red dotted line) compared to the residual hardness of the samples post-spallation using a conventional spall recovery technique, respectively.

with grain boundaries, their interactions with dislocations have been themselves the focal point of numerous studies [22,24,25]. Thus, the role these Ta clusters play as contributors to plasticity and modifying this complex NC microstructure in an improved manner has been fully established through prior work. Composition analysis of the clusters also attained via atom probe tomography has indicated the average composition of the clusters to be in the range of 32 at% Cu, 61 at% Ta, and 7 at% oxygen. The microstructure does contain a high number of grain boundaries, triple junctions, and phase boundaries, which are highlighted by colored arrows in Fig. 1. However, the microstructure has few, if any, observable dislocations/cell structures, sub-grain boundaries, twins, stacking faults, and other planar interfaces and/or voids present in the as processed state as seen in Fig. 1(A, B) and Supplemental Fig. 1. In further support of the lack of dislocations and stacking faults within the as-received material, Supplemental Fig. 1A, B has been provided. This is consistent with both experimental and simulation observations [26–29]. This is logical, given the high (ECAE) processing temperature of 700 °C, the vast majority of dislocations would have been annealed out of the Cu matrix since the recrystallization and relaxation temperature of nanocrystalline Cu is 120 °C.

To augment the *in-situ* spall results and evaluate microstructural evolution and deformation mechanisms active under extreme conditions, the NC Cu-3Ta specimens were shock compressed, allowed to undergo spallation, and then soft recovered following the procedure outlined in the experimental section. The velocity-time profiles for all *in-situ* spall experiments are shown in Fig. 2(A) and they reveal that shock compressed samples reached stable peak shock stresses ranging from 4.3 to 39.3 GPa, respectively, prior to elastic-plastic release and tensile plastic deformation, then consequent failure through spallation. In addition, the curves reveal significantly elevated HEL for the NC Cu-3Ta alloy, which was determined to be 2.0 GPa compared to 0.2–0.6 GPa for OFHC Cu [2]. In shock wave problems, it is common for shock stresses to be two or more orders of magnitude greater than the yield or flow stress of metals and metallic alloys. For most controlled shock compressed solids, the strains are found to be minimal (<5%). The Hugoniot strain can be estimated using the relationship, $\varepsilon_{11} = \frac{u_p}{U_s}$, where U_s is shock velocity and U_p is particle velocity. The shock and particle velocities derived from the limited U_s- U_p shock Hugoniot data available are determined to be 4.086 km/s and 0.291 km/s, respectively. Therefore, the Hugoniot strain at 10.9 GPa is estimated to be 0.07 or 7%. It is well known that dislocation density increases as a function of shock stress (Eq. 5) for coarse grained and single crystal metals and metallic alloys, typically well above equilibrium concentrations. Consequently, the post-shock yield stress and residual hardness comparatively increase as well. For most structures of coarse-grained metals and metallic alloys, this residual hardness exhibits an empirical linear relationship as a function of the square root of peak shock pressure/stress. This relationship has been generally represented by the empirical form stated in Eq. (6) [30,31]:

$$\sigma = \sigma_o + \alpha\mu b\sqrt{\rho} + K_1 d^{-1} + K_2 \Delta^{-1/2} \tag{5}$$

$$(\sigma - \sigma_o) = \zeta\,(H - H_o) = 2\alpha\mu b\sqrt{P} \tag{6}$$

where σ and σ_o are the post and the pre-shock yield strength, respectively, ρ is the dislocation density, K_1 and K_2 are material parameters, α is a constant $\cong$ 0.5, μ is the shear modulus, d is the dislocation cell size, Δ is the twin spacing which is negligible in NC Cu-3Ta alloys, b is the magnitude of the Burgers vector, ζ is a constant, H and H_o are the post and pre-shock hardness, and P is the peak shock pressure/stress. Both equations suggest that increasing the peak shock pressure/stress will increase the dislocation density, and consequently, the post-shock yield stress and the residual hardness. Such hardness increases have been experimentally verified in a large number of systems [2].

However, the NC Cu-3Ta alloy goes against this general trend. Fig. 2(B) shows negligible changes in the residual hardness for NC-Cu-3Ta alloys, across the through-thickness direction between the as-received material (red dotted line) and the sample shocked at a peak shock stress of 10.9 GPa. This observation holds true even when approaching the spalled surface ($\sim$ 2800 microns in Fig. 2B), where the magnitude of tensile stress is the highest. Such behavior is anomalous for metals and metallic alloys shock compressed to such high shock stresses. To the best of the author's knowledge, this type of behavior has never been reported before in the open literature for any structural materials including the work of Bringa et al. [32], which shows a significant increase in material strength as a function of shock pressure. Whereas, increases in strength of conventional coarse-grained (FCC) materials, i.e., aluminum, copper, and nickel, shocked under similar conditions to those performed in this study show significant alterations in their microstructure, be it dislocation cells/networks, stacking faults, deformation twins, and vacancy clusters [2,30,33]. For a cursory review with visual examples of the drastic changes Cu and other FCC

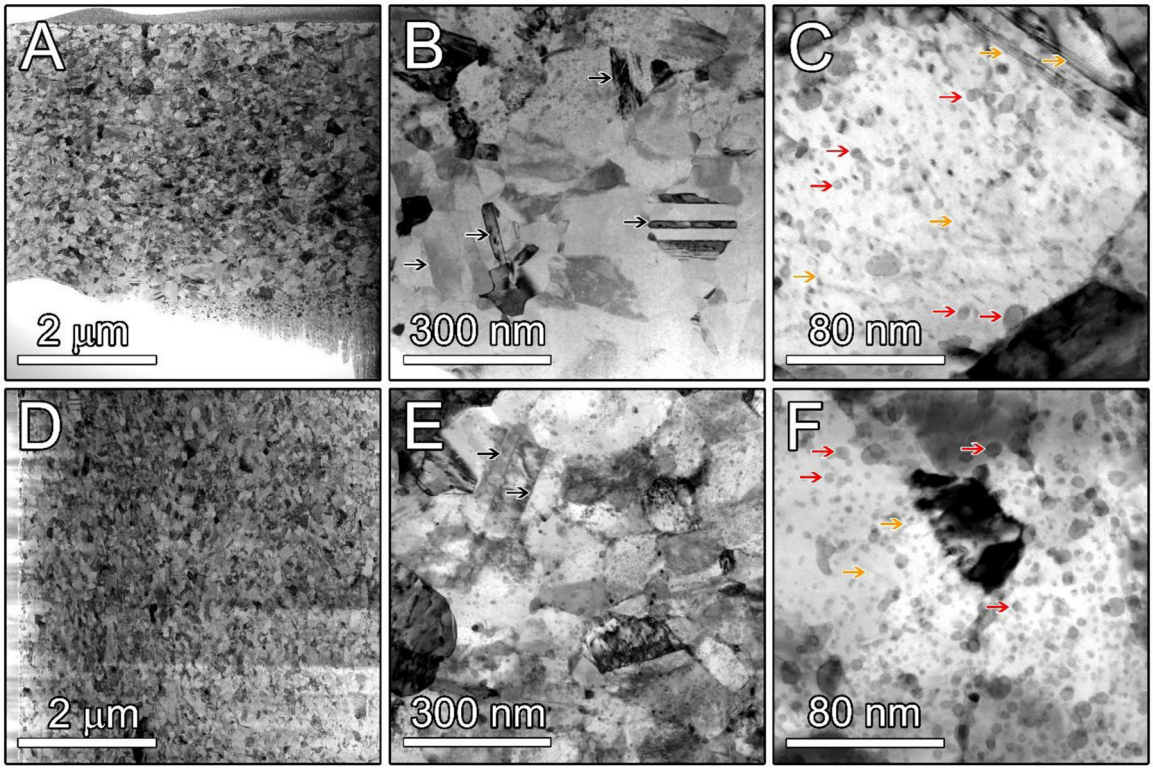

Fig. 3. STEM bright-field image after spallation, which increases in magnification: (A–C) located on the spall surface and (D–F) 320 microns away from the surface (black arrows pointing to twin boundaries, red arrows pointing to phase boundaries between Ta-based clusters and Cu matrix, and orange arrows pointing to dislocations and stacking faults).

microstructures undergo as a result of shock loading please see references [2,30,33]. The significance of the lack of shock hardening indicates stability either by maintaining a low defect density accumulation and/or absorption of defects induced under shock loading (i.e. initial compression and tensile loading) due to an inherently stable microstructure. This is consistent with earlier findings on shock-recovered samples as well as other works on this system [18,19,34–37].

To further address the role of stable microstructure after shock loading, Fig. 3 provides low and high magnification bright-field STEM micrographs of the spall recovered sample shocked to ~10.9 GPa (~600 m/s). Two regions of interest were investigated, the first region is along the proximity of the spall surface (Fig. 3(A–C)) and the second is along approximately 320 microns away from the spall surface (Fig. 3(D–F)). These two regions were selected, based on the estimated width of the spall plane, with the first being located closest to the region experiencing the highest tensile stress and the second region located away from the spall plane where the tensile stress has dissipated to a lower value. The full TEM lift out for the sample taken directly next to the fracture surface is provided in Supplemental Fig. 2, showing ~32 μm^2 of electron transparency. Based on the analysis of the residual microstructure of NC Cu-3Ta post spallation, it is apparent that only a marginal change in the average grain size was observed between the as-received and spall recovered samples, being 100 and 118 nm, respectively, a 18% increase in grain size. Additionally and more importantly, no increase in dislocation density and mechanical twinning is observed, i.e., stabilized NC alloys likely exhibit an unprecedented ability to resist high defect (such as dislocation) accumulation and damage. The limited number of these defects observed in the microstructures were pointed out using color arrows as described in the figure caption. Theses defects were observed to be present only within the limited number of grains having much large grain sizes, double to triple, the average grain size (100 nm). Additionally for more images of the limited number of dislocations and stacking faults, please see Supplemental Fig. 1C, D Such resistance has not been observed before and is analogous to the ability of NC metals to absorb radiation damage, where stable interfaces act as potent sinks for point defects [34,38].

Here, in the same way, the thermo-mechanically stabilized grain boundaries and cluster interfaces persist and continue to operate as sinks to absorb the deformation defects. That is, the authors have previously reported that dislocations in NC Cu-Ta alloys can emit from the grain boundaries during the deformation process, but they may be absorbed back into neighboring grain boundary regions and may not extend far into the grain interiors or pile up, leading to negligible changes in the defect density and hence, residual hardness [22,36,39]. Such inherent behavior or properties are unlikely to be observed in un-stabilized NC metals, where their microstructures would become unstable under the intensified driving force, i.e., as the microstructure evolves, the sink density reduces [35]. Therefore, the resilient phenomena of absorbing defects and resisting microstructural evolution under extreme dynamic conditions, as reported here, is only possible in thermo-mechanically stabilized NC metals, such as this NC Cu-3Ta alloy. This ability to absorb damage is a coupled effect between the grain boundaries and Ta clusters. The reason why these two effects cannot be decoupled is that the grain volume is preserved under the high stresses induced during shock loading. This is only due to the pinning effect provided by the high density and stability of the Ta clusters. In general, the accumulation of defects during shock compression can lead to an increase in potential void nucleation sites such as vacancies and vacancy clusters, which are detrimental to spall failure [2,40]. On the contrary, the actual experimental results show an opposite trend. To this note, Fig. 4 provides the spall strength map of various alloys as a function of melting tempera-

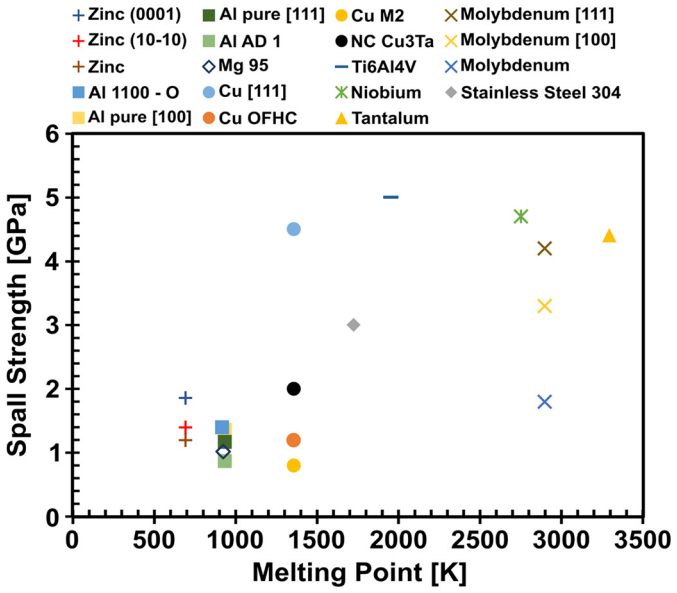

Fig. 4. Spall strength as a function of melting point map for various metals including alloys and single crystals.

ture, including that of NC Cu-3Ta alloy. Interestingly, the NC Cu-3Ta alloy show about a 2-fold increase as compared to coarse-grained OFHC Cu [2]. While this spall strength value represents a significant improvement, the question remains as to why is the spall strength of NC Cu-3Ta not much higher, i.e. more closely approaching the strength of single-crystal (4.5 GPa) [2].

The experimental results discussed above demonstrate the impact of NC Cu-3Ta alloy microstructure on the spall strength. For shock-loaded polycrystalline materials, failure occurs at several microstructure levels with the elementary carrier of failure having traditionally been dominated by grain and phase boundaries. These microstructural features prevail in defining many material properties including the spall strength albeit spall strength is not considered to be an intrinsic material property. In NC Cu-Ta alloys, the addition of Ta tends to improve the cohesive strength of its grain boundaries. For instance, using atomistic simulations combined with high-resolution TEM experiments, Frolov et al. [28] showed that the presence of Ta solute in Cu grain boundaries would subsequently increase the cohesive energy, indicative of structural stability as well as strength compared to pure Cu and its alloys. This increase in the cohesive strength will greatly hamper void nucleation processes at the GB during shock loading. Further, the Ta nanoclusters that are decorated along the grain boundaries, as well as grain interiors, pin the GBs in place, i.e., controlling the GB deformation processes such as sliding and rotation during creep by the Zener pinning mechanism [41–48]. The lack of sliding and rotation observed in these grain boundaries indicate they are more resistant to deformation, and therefore, less likely to nucleate and grow voids during the tensile loading phase or spallation.

It should be noted that the interaction of these clusters with dislocations and grain boundaries accounts for 60–70 percent of the alloy's apparent strengthening [39]. That is, most of the strength comes from non-planar defects, whose dimensional length scale is far less than the shock width ~ 50 nm and are coherent to semi-coherent with the matrix [39] and therefore, are less likely to have observable interactions with propagating shock waves. Prior simulations and experiments by the authors have shown that the spatial distribution of Ta-based clusters in NC-Cu-Ta alloys effectively pin and limits the steady-state velocity of gliding dislocations during high strain rates loading conditions but below those observed in shock loading [36,49]. This restriction of dislocation velocity was shown to be a key contributor to the high rate mechanism of phonon drag, i.e., the mechanism of phonon drag was shown to be suppressed and completely damped out up to strain rates of 10^5 s^{-1} [36] (more on this below). Since NC Cu-Ta alloys do not exhibit the same upturn in flow stress at strain rates between 10^3 and 10^4 s^{-1} (due to an increase in hardening) compared to traditional metals and alloys, they should be able to absorb high rate deformation more efficiently by deforming in a more ductile manner at extreme strain rates as has been previously observed in similar NC Cu-Ta systems at strain rates below the shock regime [36]. This suggests that NC Cu-3Ta should exhibit higher spall strengths than conventional polycrystalline microstructures. However, since the entire volume of defects first undergoes compression, in particular those within the spall plane where the tensile stress is maximum, the failure process shifts from the traditionally weakest microstructural features such as grain boundaries and Ta-based cluster interfaces to the large incoherent Ta/Cu interfaces. Such planar interfaces of secondary phases (i.e. interfaces whose dimensional length-scale is far greater than the shock width ~ 50 nm) fail under shock loading due to the three main reasons given in the introduction. Fig. 5 reveals this transition, that is, below some critical lower length-scale, features including grain and phase boundaries do not contribute to the failure process thereby explaining the enhanced spall strength observed.

Overall, the fractography of the fully spalled surface indicates a generally ductile morphology. That is, regions exist where microvoids have grown and coalesced forming well-defined dimpled regions as shown in Fig. 5(A, B). The dimples are on average 1 μm in diameter. This indicates that hundreds of grains were involved in the local void growth process, which occurs via shearing, necking, and coalescence of adjacent smaller micro-cavities. Inside larger dimples, it is clearly evident that the void nucleation process was initiated by the brittle failure of micron-sized Ta particles. Specifically, Fig. 5(B–D) reveals where large Ta particles were cleaved or shattered, and debonded from the Cu matrix post-spallation. This is interesting as one would expect brittle intermetallic phases to undergo this type of failure; however, Ta is an exceptionally ductile metal, similar in nature to Cu despite its extremely high melting point. That is, both Ta and Cu exhibit the ability to undergo ~80% cross-sectional area reduction in conventional tensile loading at room temperature [50,51]. However, given their incoherent nature, the large difference in density and sound speed between the Cu matrix and Ta particle leads to a significant impedance mismatch at the interface. Such high impedance mismatch will result in partial reflection and transmission at the Cu matrix and Ta particle interface. Collisions between the reflection from the interface and the release wave from the primary shock pulse may result in tensile waves of strong magnitude and consequently, leads to cavitation and separation at these weak interfaces as revealed in Fig. 5(B–D). From the cross-sections along the spall plane, numerous voids can be identified initiating at these interfaces. These voids are the origin of spall failure as they grow and coalesce to form macro-cracks along the spall plane. Such effects are much less likely to occur at the interface of the matrix with the coherent/semi-coherent Ta-based clusters as their density based on composition and lattice matching with the matrix would significantly lessen the expected impedance mismatch. This is supported by the lack of these types of microstructural features being present in the TEM observations taken within the spall plane of the sample (see Fig. 5(E–P)).

Fig. 5(E–L) highlights the spallation and crack formation within the large Ta particle and the interface between it and the Cu matrix. Fig. 5(E) shows a low magnification bright field image of a large Ta particle fractured completely into two separate halves. Fig. 5(F) is the area ascribed by the red box in Fig. 5(E) and

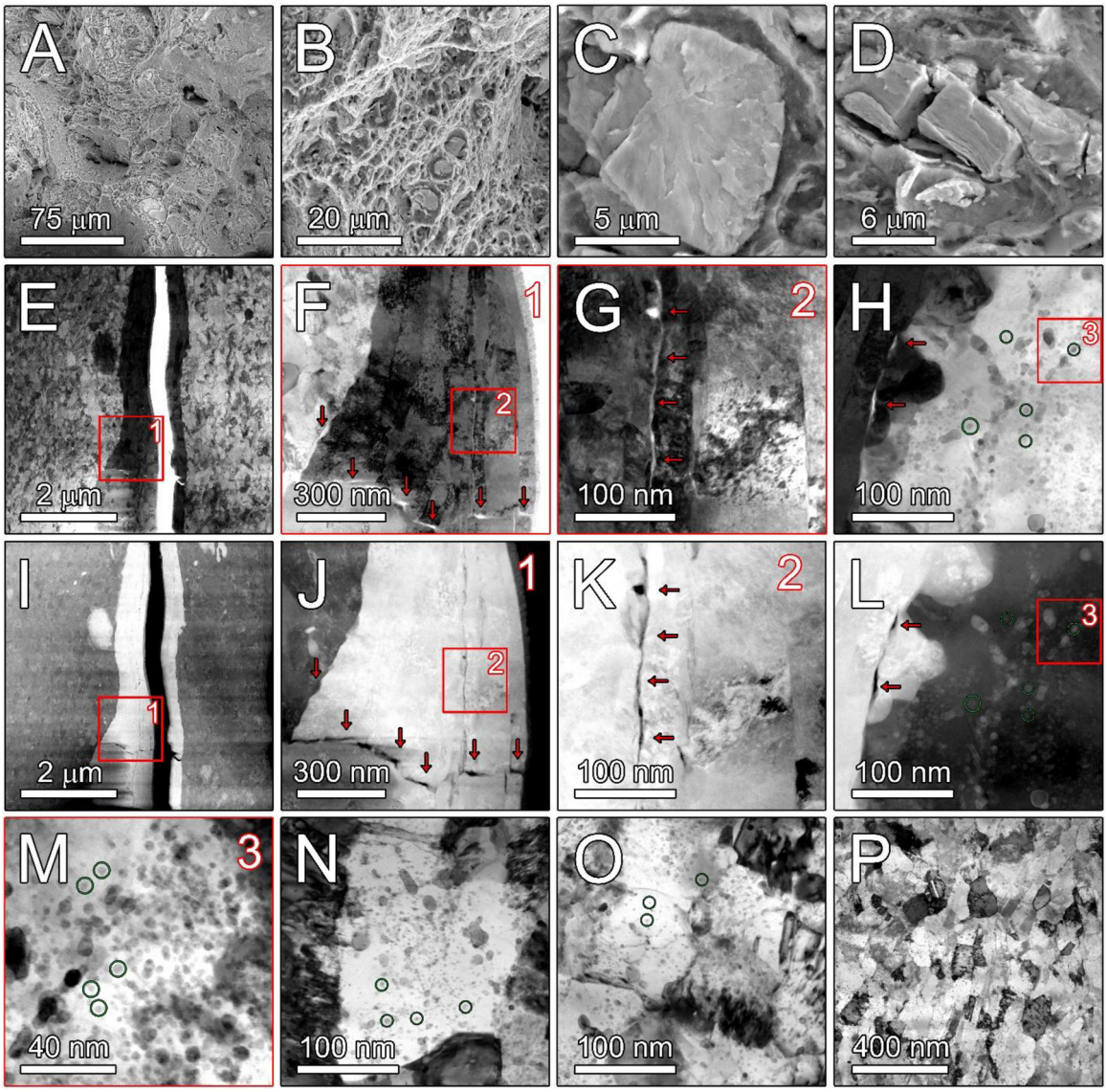

Fig. 5. Fracture and failure of NC Cu–3Ta alloy shock loaded to 10.9 GPa: (A–D) secondary electron scanning electron microscopy (SEM) images of the fracture surface with increasing magnification. Fig. (C, D) are high magnification images of larger Ta particles that are cleaved or shattered by interacting with the shock wave. Fig. (E–H) and (I–L): STEM bright-field and HAADF images after spallation, with an increase in magnification. Red arrows point to regions of fracture and separation occurring in or around the larger Ta particles. Fig. (M–P) STEM bright-field images after spallation, with a decrease in magnification. Green circles are used to identify individual coherent and semi-coherent Ta clusters within the Cu matrix. The STEM images were taken from the lift-out specimen taken perpendicular to the spall surface. The small inset boxes with numbering shows the region of interest shown in neighboring higher magnification image for which it originated. For example, the small inset box #1 in image E corresponds to image F.

provides a higher magnification image clearly showing numerous nano-fractures within the particle. It should be noted that the Ta particle has thin, low-angle, planar grains that are several microns in length by roughly 100 nm in width and orientated normal to the shock direction. Fig. 5(G) (blown up image from the orange box in Fig. 5(F)) illustrates the effect the shock wave had on void nucleation and dynamic fracture along these planar grain boundaries. Fig. 5(H) captures the nucleation and fracture between the large Ta particle and the interface with the Cu matrix. Despite this region undergoing a triaxial state of stress, it should be noted that the small coherent/semi-coherent boundaries do not show any signs of void nucleation or debonding with the matrix. An even higher magnification bright field with a high density of these coherent/semi-coherent particles taken from within the area of Fig. 5(H, L) shows no sign or evidence of void nucleation or fracture of these types of interfaces. Moving out sequentially to a more macro-view of the microstructure (Fig. 5(N–P)), no signs of voids or fractures are observed along the grain boundaries or within the grain interiors. One observation that can be made is that, in grains substantially larger than the average Cu grain size; a low density of dislocations can be observed interacting and being pinned by arrays of Ta clusters. To summarize the TEM results, the smaller coherent/semi-coherent ($<$ 15.6 nm) Ta particles, as well as the nanocrystalline grain boundaries of the Cu matrix, do not exhibit any evidence of void nucleation, debonding, or fracture contrary to prior modeling work [13,52]. While the disparity between the modeling and experimental work is interesting, it does point to more work being needed to rectify the inconsistencies between the modeling efforts and experimental observations. One possible explanation is that the models are likely overdriven due to time and length scale issues.

From the above analysis, the atomic clusters were determined to be smaller than the width of the propagating shock wave, which is in contrast to conventional alloys for which the precip-

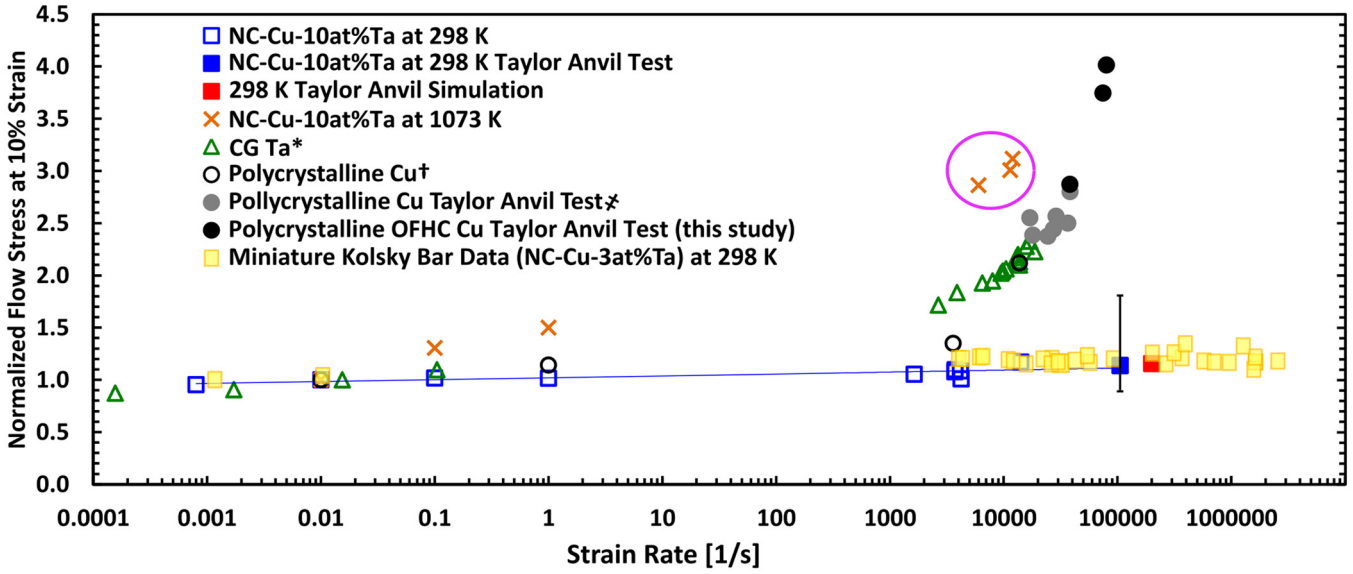

Fig. 6. Normalized flow stress as a function of strain rate and temperature. NC Cu-3Ta under ambient conditions and 1073 K compared to high-purity coarse-grained Cu and Ta. As well as (OFHC) Cu tested by Taylor anvil experiment and miniature Kolsky bar data at ambient conditions. The power-law fit for the NC-Cu-3Ta data reveals that the material is subjected primarily to thermal activation processes up to a strain rate of at least 2.4×10^6 s^{-1}.

itated phases are orders of magnitude larger. For example, nucleation of voids was observed along with planar interfaces, Ta interfaces $>$ 500 nm. We define planar interfaces as an interface whose dimensional length is an order of magnitude greater than the width of the shock front, $\sim$ 50 nm. These observed differences can be correlated to the strain rate insensitivity of the NC Cu-Ta alloy relative to the coarser-grained constituent counterparts of its composition, i.e., pure Ta and pure Cu as shown in Fig. 6. Again, prior work has delineated the effect microstructural length scales can have on tuning, damping, and/or removing the phonon-drag effect and thus strain-rate sensitivity under dynamic loading for NC Cu-Ta alloys [36,37,49].

To further understand the shock response of NC Cu-Ta, Fig. 6 provides the flow stress results for NC-Cu-3Ta alloy at a constant plastic strain of 10%, which are normalized with the 10% flow stress obtained from the same temperature at a strain rate of 10^{-2} s^{-1} then plotted as a function of strain rate. The normalized flow-stress data for polycrystalline Cu, polycrystalline Ta, and coarse-grained oxygen-free high conductivity Cu obtained by Taylor anvil experiments and those reported in reference [36] are also presented. In addition, a series of miniature Kolsky bar data has been plotted up to a strain rate of 2.4×10^6 s^{-1}. In general, these strain rates are lower than those experienced in shock compression but provide a critical understanding of materials response. For instance, a clear upturn in the flow stress, albeit initiating at differing strain rates, can be noted for polycrystalline Cu and Ta. The observed dramatic rise in flow stress (or loss in ductility) is fundamental in origin, and therefore, common to many structural metals such as Cu, Ni, and Ta. This upturn is believed to be the direct result of the rise in the mobile dislocation drag force brought about by interactions with phonons in the crystal lattice and some heavily deformed coarse-grained samples due to an increase in the dislocation density. More recently, data was published showing that below a certain length scale ($<$ 150 nm) [36,49], the Cu-Ta system becomes insensitive to strain rate and deforms along the same lines as if it was quasi-statically deformed (see Fig. 6). Namely, it does not undergo the rapid upturn in flow stress and embrittling failure behavior synonymous with phonon drag. That is, while an average grain size i.e. that of $\sim$ 100 nm for Cu-Ta alloys, has been shown to yield a physical activation volumes between 40 and $60b^3$, the strain rate sensitivity of these alloys are controlled by the cluster spacing [39,49,53,54]. It was previously determined that the cluster spacing ranges from 4 to 8 nm, which is an order of magnitude smaller than average grain size diameter [26,36]. Under these conditions, a dislocation can be nucleated, but becomes instantly pinned thereafter i.e., a dislocation cannot accelerate to a steady-state velocity high enough to interact with phonons within the lattice and induce the so-called phonon drag effect (thereby exhibiting negligible strain rate sensitivity) [36,49]. Further, previous works, have shown that once dislocations are pinned by Ta clusters, they can be reabsorbed by neighboring grain boundaries [22,39]. Here it should be noted, that as the sample temperature is increased to 1073 K for the NC Cu-Ta alloy as revealed in Fig. 6 by data points marked as “X”, a notable increase in the strain rate sensitivity is observed due to phonon-drag effects. The drag coefficient associated with phonon drag is temperature-dependent and can be directly correlated to the phonon density of states, which also increases with temperature. Due to this relation, there is a much larger dislocation/phonon drag effect in the sample tested at elevated temperatures as compared to samples tested at lower temperatures. Additional follow-on work revealed that through tuning length scale features, (grain size and cluster spacing), it is possible to control the degree to which phonon drag manifests itself in Cu-Ta alloys [49]. Explicitly, below a critical length scale phonon drag was shown be be damped out, however, as this length scale was relaxed, became larger in dimention, increasingly higher strain rate sensitivity with more bittle behavior was observed [49]. Similarly, as shown here, planar interfaces, i.e. coarser-grained material (Fig. 6), where the length scale is $\gg$ 100 nm, does undergo this embrittling effect despite being ductile under quasi-static conditions of tension and compression loading [4,9]. Thus, this may explain why the SEM images capture a ductile fracture within the Cu matrix, whereas the Ta particles show cleavage or brittle fracture, despite tantalum’s inherent ductile nature.

Fig. 7 provides composite optical micrographs of NC Cu-3Ta having undergone incipient spall and for reference, complete spallation (peak shock stress of 5.5 and 10.9 GPa, respectively). In both cases (Fig. 7(A, B)), the spall pattern is atypical, i.e., it exhibits multiple isolated cracks in a wide region, which are meandering in character and is not typical of spall planes generally

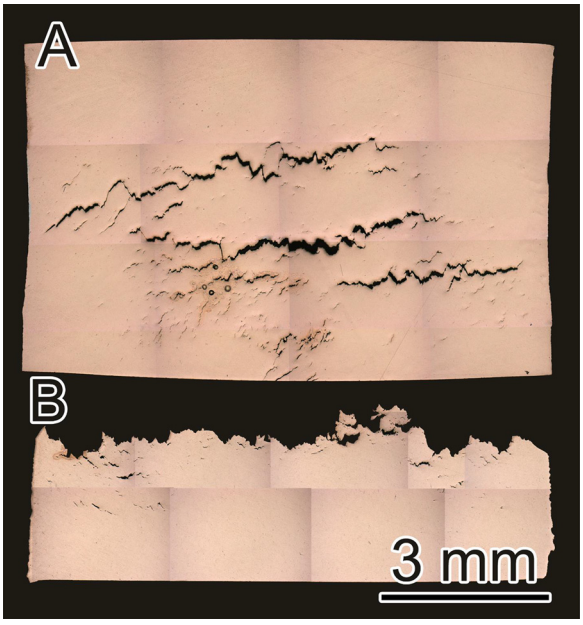

Fig. 7. Optical cross-sections composite images of spalled NC Cu-3Ta samples (A) incipient (peak stress of 5.5 GPa) and (b) complete spall (peak stress of 10.9 GPa).

observed in ductile metals and metallic alloys. Spallation in metals and metallic alloys generally occurs along a single well-defined plane. This spall pattern may be indicative of the material's ability to disperse energy. In particular, the numerous spall planes, as well as much smaller fracture sites, i.e., nano-fractures, dispersed throughout the sample volume shown in Fig. 7(A), suggest that the fracture is dominated by void nucleation, growth, and coalescence. Given that the entire volume of larger incoherent Ta particles randomly dispersed throughout the volume of the sample is subjected to loading, the cracks nucleate heterogeneously. However, as seen in Fig. 7(B), i.e., at higher shock stress, failure appears to be dominated more by the growth of cracks initated at Ta particles particles as opposed to nucleation a high density of cracks. Further, since the localization of fracture is decreased (as shown in Fig. 7(A, B)) along with an increase in the overall width of the spall plane points towards an increase in the velocity dispersion. Generally, the greater the meso-particle velocity dispersion is the greater a material's ability to relieve micro-stresses is and thus leads to greater spall strength. During the impact loading, micro-stresses in the material decrease due to relaxation processes (heterogeneous microstructures) revealing the higher spall strength.

In other words, shock wave propagation through solids requires that the entire volume, including its defects, will undergo shock compression. The failure process is a probability of void nucleation, growth, and coalescence occurring within this volume of defects. The vast majority of defects, grain boundaries, and phase boundaries in NC Cu-Ta do not contribute to the void nucleation and growth processes. The presence of the grain boundary volume absorbs the vast majority of defects during the shock compression phase. Therefore, during spallation, the tensile wave only interacts with the limited volume of these large incoherent Ta particles because of their limited presence due to the low solute content of NC Cu-3Ta. This is visually confirmed by observing Supplemental Fig. 2, where only one large Ta particle ($\sim$ 500 nm in length) is present within an area of $\sim$ 32 μm^2. Thus, if a nano-crack nucleates within the Ta particle (Fig. 5(J, K)), it would require a large enough stress to propagate and grow. Furthermore, given the strain-rate insensitivity and plasticity within the Cu matrix to relieve stress and strain around these isolated fractured particles, this prolongs fracture from occurring by requiring higher stress to grow those limited features to a critical flaw size. This is supported by the SEM micrographs (Fig. 5A–D) showing cleaved Ta particles that are surrounded by dimpled regions of the Cu matrix. However, more fundamental research is needed to address the role of mechanical processing parameters to improve the spall strength of NC Cu-3Ta alloys. If mechanical processing of NC Cu-3Ta alloys could be improved to remove all large incoherent Ta particles and precipitates leaving only atomic clusters in the microstructure, the material may exhibit spall strengths more in line with single crystals.

4. Conclusions

In this work, the shock, damage, and failure behavior of a bulk, stable NC Cu-3Ta alloy was probed to elucidate the anomalous response of this nanocrystalline material under extreme dynamic conditions. Time-resolved *in-situ* and spall recovery experiments were employed for this study. The bulk, stable NC Cu-3Ta alloy samples were shock compressed to stresses ranging from 4.3 to 39.3 GPa, respectively, and advanced microstructural characterization techniques were used to study damage nucleation and accumulation as they relate to deformation mechanisms. The results reveal a significantly high HEL (2.0 GPa) and spall strength (1.19–1.67 GPa) compared to OFHC Cu along with negligible changes in the residual hardness and microstructure of the shock recovered sample. The measured spall strength of this NC Cu-Ta alloy exhibits approximately a 2x increase compared to polycrystalline Cu. Further, STEM characterization indicates no increase in dislocation density and mechanical twinning after shock loading, i.e., stabilized NC alloys likely exhibit an unprecedented ability to resist high defect (such as dislocation) accumulation and damage. This anomalous behavior in stable NC Cu-3Ta alloy can be attributed to the elimination/limitation of defects formed under shock conditions coupled with a divergent strain-rate-insensitive behavior of its main microstructural features. Overall, the present work highlights the fact that if designed properly, some critical lower length-scale features including grain and phase boundaries may not contribute to the failure process thereby enhancing the spall strength. However, more fundamental research is needed to address the role of processing parameters that could lead to a material with superior spall strengths being more in line with single crystals. This research should serve as a starting point for the materials in a dynamic environment community and perhaps, will open the door for further research studies into the exact atomic-scale mechanisms at play.

Declaration of Competing Interest

The authors declare that they have no known competing financial interests or personal relationships that could have appeared to influence the work reported in this paper.

Acknowledgements

The authors acknowledge A.J Roberts and T. Luckenbaugh for the synthesis of the Cu-Ta powder; T. Luckenbaugh, S. Marsh, and M.C. Aniska for consolidation of the Cu-Ta powder and machining. Also, the authors are grateful to E. Wilson, D. Ayers, and J. Bradley for their support in conducting the shock experiments. K.S. acknowledges the Support of the DEVCOM Army Research Laboratory and the National Science Foundation under contracts W911NF-15-2-0038 and 1663287. The authors would also like to thank Prof. Naresh Thadhani from Georgia Tech for very insightful conversations and suggestions related to the content of this paper.

Supplementary materials

Supplementary material associated with this article can be found, in the online version, at doi:10.1016/j.actamat.2022.118105.

References

[1] M.A. Meyers, Dynamic Behavior of Materials, John wiley & sons, 1994.
[2] C.L. Williams, Structure-property relationships under extreme dynamic environments: shock recovery experiments, Synth. SEM Lect. Exp. Mech. 2 (2019) 1–155, doi:10.2200/S00880ED1V01Y201810SEM004.
[3] M.A. Meyers, L.E. Murr, K.P. Staudhammer, in: Shock-wave and high-strain-rate phenomena in materials. CRC, 1992.
[4] R.W. Minich, J.U. Cazamias, M. Kumar, A.J. Schwartz, Effect of microstructural length scales on spall behavior of copper, Metall. Mater. Trans. A 35 (2004) 2663–2673, doi:10.1007/s11661-004-0212-7.
[5] E.O. Hall, The deformation and ageing of mild steel: III discussion of results, Proc. Phys. Soc. Sect. B 64 (1951) 747, doi:10.1088/0370-1301/64/9/303.
[6] N. Petch, The cleavage strength of polycrystals, J. Iron Steel Inst. 174 (1953) 25–28.
[7] M.A. Meyers, K.K. Chawla, Mechanical Behavior Materials, 2nd ed. 2nd-edition, Cambridge University Press, United Kingdom, 2008 http://www.cambridge.org/us/academic/subjects/engineering/materials-science/mechanical-behavior-materials (accessed May 24, 2017).
[8] S.V. Razorenov, G. Garkushin, G.I. Kanel, O.N. Ignatova, The spall strength and Hugoniot elastic limit of tantalum with various grain size, AIP Conf. Proc. 1426 (2012) 991–994, doi:10.1063/1.3686444.
[9] T. Chen, Z.X. Jiang, H. Peng, H.L. He, L.L. Wang, Y.G. Wang, Effect of grain size on the spall fracture behaviour of pure copper under plate-impact loading, Strain 51 (2015) 190–197, doi:10.1111/str.12132.
[10] P. Peralta, S. DiGiacomo, S. Hashemian, S.N. Luo, D. Paisley, R. Dickerson, E. Loomis, D. Byler, K.J. Mcclellan, H. D'Armas, Characterization of incipient spall damage in shocked copper multicrystals, Int. J. Damage Mech. 18 (2009) 393–413, doi:10.1177/1056789508097550.
[11] J.P. Escobedo, D. Dennis-Koller, E.K. Cerreta, B.M. Patterson, C.A. Bronkhorst, B.L. Hansen, D. Tonks, R.A. Lebensohn, Effects of grain size and boundary structure on the dynamic tensile response of copper, J. Appl. Phys. 110 (2011) 033513, doi:10.1063/1.3607294.
[12] T.P. Remington, E.N. Hahn, S. Zhao, R. Flanagan, J.C.E. Mertens, S. Sabbaghianrad, T.G. Langdon, C.E. Wehrenberg, B.R. Maddox, D.C. Swift, B.A. Remington, N. Chawla, M.A. Meyers, Spall strength dependence on grain size and strain rate in tantalum, Acta Mater. 158 (2018) 313–329, doi:10.1016/j.actamat.2018.07.048.
[13] J. Chen, M.A. Tschopp, A.M. Dongare, Shock wave propagation and spall failure of nanocrystalline Cu/Ta alloys: effect of Ta in solid-solution, J. Appl. Phys. 122 (2017) 225901, doi:10.1063/1.5001761.
[14] A.M. Dongare, A.M. Rajendran, B. LaMattina, M.A. Zikry, D.W. Brenner, Atomic scale studies of spall behavior in nanocrystalline Cu, J. Appl. Phys. 108 (2010) 113518, doi:10.1063/1.3517827.
[15] J. Chen, S.N. Mathaudhu, N. Thadhani, A.M. Dongare, Unraveling the role of interfaces on the spall failure of Cu/Ta multilayered systems, Sci. Rep. 10 (2020) 1–15, doi:10.1038/s41598-019-57048-9.
[16] F. Wang, Y. Liu, T. Zhu, Y. Gao, J. Zhao, Nanoscale interface of metals for withstanding momentary shocks of compression, Nanoscale 2 (2010) 2818–2825, doi:10.1039/C0NR00333F.
[17] E.N. Borodin, A.E. Mayer, Theoretical interpretation of abnormal ultrafine-grained material deformation dynamics, Model. Simul. Mater. Sci. Eng. 24 (2016) 025013, doi:10.1088/0965-0393/24/2/025013.
[18] B.C. Hornbuckle, C.L. Williams, S.W. Dean, X. Zhou, C. Kale, S.A. Turnage, J.D. Clayton, G.B. Thompson, A.K. Giri, K.N. Solanki, K.A. Darling, Stable microstructure in a nanocrystalline copper–tantalum alloy during shock loading, Commun. Mater. 1 (2020) 1–6, doi:10.1038/s43246-020-0024-3.
[19] B.C. Hornbuckle, S.W. Dean, X. Zhou, A.K. Giri, C.L. Williams, K.N. Solanki, G.B. Thompson, K.A. Darling, Laser shocking of nanocrystalline materials: Revealing the extreme pressure effects on the microstructural stability and deformation response, Appl. Phys. Lett. 116 (2020) 231901, doi:10.1063/5.0008107.
[20] S. Razorenov, G. Kanel, The strength of copper single crystals and the factors governing metal fracture in uniaxial dynamic stretching, Phys. Met. Metallogr. 74 (1992) 526–530.
[21] T. Antoun, L. Seaman, D.R. Curran, G.I. Kanel, S.V. Razorenov, A.V. Utkin, Spall Fracture, Springer Science & Business Media, 2003.
[22] C. Kale, S. Srinivasan, B.C. Hornbuckle, R.K. Koju, K. Darling, Y. Mishin, K.N. Solanki, An experimental and modeling investigation of tensile creep resistance of a stable nanocrystalline alloy, Acta Mater. 199 (2020) 141–154, doi:10.1016/j.actamat.2020.08.020.
[23] B.C. Hornbuckle, K. Solanki, K.A. Darling, Prolonged high-temperature exposure: tailoring nanocrystalline Cu–Ta alloys against grain growth, Mater. Sci. Eng. A 824 (2021) 141818, doi:10.1016/j.msea.2021.141818.
[24] M. Bhatia, M. Rajagopalan, K. Darling, M. Tschopp, K. Solanki, The role of Ta on twinnability in nanocrystalline Cu–Ta alloys, Mater. Res. Lett. 5 (2017) 48–54.
[25] K.A. Darling, M. Rajagopalan, M. Komarasamy, M.A. Bhatia, B.C. Hornbuckle, R.S. Mishra, K.N. Solanki, Extreme creep resistance in a microstructurally stable nanocrystalline alloy, Nature 537 (2016) 378–381, doi:10.1038/nature19313.
[26] M. Rajagopalan, K. Darling, S. Turnage, R. Koju, B. Hornbuckle, Y. Mishin, K. Solanki, Microstructural evolution in a nanocrystalline Cu-Ta alloy: a combined *in-situ* TEM and atomistic study, Mater. Des. 113 (2017) 178–185.
[27] K.A. Darling, A.J. Roberts, Y. Mishin, S.N. Mathaudhu, L.J. Kecskes, Grain size stabilization of nanocrystalline copper at high temperatures by alloying with tantalum, J. Alloy. Compd. 573 (2013) 142–150.
[28] T. Frolov, K.A. Darling, L.J. Kecskes, Y. Mishin, Stabilization and strengthening of nanocrystalline copper by alloying with tantalum, Acta Mater. 60 (2012) 2158–2168, doi:10.1016/j.actamat.2012.01.011.
[29] B.C. Hornbuckle, T. Rojhirunsakool, M. Rajagopalan, T. Alam, G.P.P. Pun, R. Banerjee, K.N. Solanki, Y. Mishin, L.J. Kecskes, K.A. Darling, Effect of Ta solute concentration on the microstructural evolution in immiscible Cu-Ta alloys, JOM 67 (2015) 2802–2809, doi:10.1007/s11837-015-1643-x.
[30] L.E. Murr, M.A. Meyers, L.E. Murr, Residual microstructure - mechanical property relationships in shock-loaded metals and alloys, in: Shock Waves High-Strain-Rate Phenomena Metals: Concepts and Applications, Springer US, Boston, MA, 1981, pp. 607–673, doi:10.1007/978-1-4613-3219-0_37.
[31] L.E. Murr, M.A. Meyers, L.E. Murr, Effects of peak pressure, pulse duration, and repeated loading on the residual structure and properties of shock deformed metals and alloys, in: Shock Waves High-Strain-Rate Phenomena Metals: Concepts and Applications, Springer US, Boston, MA, 1981, pp. 753–777, doi:10.1007/978-1-4613-3219-0_42.
[32] E.M. Bringa, A. Caro, Y. Wang, M. Victoria, J.M. McNaney, B.A. Remington, R.F. Smith, B.R. Torralva, H.V. Swygenhoven, Ultrahigh strength in nanocrystalline materials under shock loading, Science 309 (2005) 1838–1841, doi:10.1126/science.1116723.
[33] C.L. Williams, C.Q. Chen, K.T. Ramesh, D.P. Dandekar, On the shock stress, substructure evolution, and spall response of commercially pure 1100-O aluminum, Mater. Sci. Eng. A 618 (2014) 596–604, doi:10.1016/j.msea.2014.09.030.
[34] S. Srinivasan, C. Kale, B.C. Hornbuckle, K.A. Darling, M.R. Chancey, E. Hernández-Rivera, Y. Chen, T.R. Koenig, Y.Q. Wang, G.B. Thompson, K.N. Solanki, Radiation tolerance and microstructural changes of nanocrystalline Cu-Ta alloy to high dose self-ion irradiation, Acta Mater. 195 (2020) 621–630, doi:10.1016/j.actamat.2020.05.061.
[35] B.C. Hornbuckle, C. Kale, S. Srinivasan, T.L. Luckenbaugh, K.N. Solanki, K.A. Darling, Revealing cryogenic mechanical behavior and mechanisms in a microstructurally-stable, immiscible nanocrystalline alloy, Scr. Mater. 160 (2019) 33–38, doi:10.1016/j.scriptamat.2018.09.035.
[36] S.A. Turnage, M. Rajagopalan, K.A. Darling, P. Garg, C. Kale, B.G. Bazehhour, I. Adlakha, B.C. Hornbuckle, C.L. Williams, P. Peralta, K.N. Solanki, Anomalous mechanical behavior of nanocrystalline binary alloys under extreme conditions, Nat. Commun. 9 (2018) 2699, doi:10.1038/s41467-018-05027-5.
[37] D. Casem, J. Ligda, T. Walter, K. Darling, B. Hornbuckle, Strain-rate sensitivity of nanocrystalline Cu–10Ta to 700,000/s, J. Dyn. Behav. Mater. (2019), doi:10.1007/s40870-019-00223-w.
[38] S. Srinivasan, B.C. Hornbuckle, K.A. Darling, H. Kim, Y.Q. Wang, K. Solanki, Helium partitioning to the core-shelled Ta nanoclusters in nanocrystalline Cu-Ta alloy, Scr. Mater. 208 (2022) 114344, doi:10.1016/j.scriptamat.2021.114344.
[39] C. Kale, S. Turnage, P. Garg, I. Adlakha, S. Srinivasan, B.C. Hornbuckle, K. Darling, K.N. Solanki, Thermo-mechanical strengthening mechanisms in a stable nanocrystalline binary alloy – a combined experimental and modeling study, Mater. Des. 163 (2019) 107551, doi:10.1016/j.matdes.2018.107551.
[40] H. Kressel, N. Brown, Lattice defects in shock-deformed and cold-worked nickel, J. Appl. Phys. 38 (1967) 1618–1625, doi:10.1063/1.1709733.
[41] F. Abdeljawad, P. Lu, N. Argibay, B.G. Clark, B.L. Boyce, S.M. Foiles, Grain boundary segregation in immiscible nanocrystalline alloys, Acta Mater. 126 (2017) 528–539, doi:10.1016/j.actamat.2016.12.036.
[42] E. Nes, N. Ryum, O. Hunderi, On the Zener drag, Acta Metall. 33 (1985) 11–22, doi:10.1016/0001-6160(85)90214-7.
[43] W.-B. Li, K.E. Easterling, The influence of particle shape on Zener drag, Acta Metall. Mater. 38 (1990) 1045–1052, doi:10.1016/0956-7151(90)90177-I.
[44] P.A. Manohar, M. Ferry, T. Chandra, Five decades of the Zener equation, ISIJ Int. 38 (1998) 913–924, doi:10.2355/isijinternational.38.913.
[45] M. Miodownik, E.A. Holm, G.N. Hassold, Highly parallel computer simulations of particle pinning: Zener vindicated, Scr. Mater. 42 (2000) 1173–1177, doi:10.1016/S1359-6462(00)00354-7.
[46] C.L.D. Prinzio, E. Druetta, O.B. Nasello, More about Zener drag studies with Monte Carlo simulations, Model. Simul. Mater. Sci. Eng. 21 (2013) 025007, doi:10.1088/0965-0393/21/2/025007.
[47] R.K. Koju, K.A. Darling, L.J. Kecskes, Y. Mishin, Zener pinning of grain boundaries and structural stability of immiscible alloys, JOM (2016) 1–9, doi:10.1007/s11837-016-1899-9.
[48] R.K. Koju, K.A. Darling, K.N. Solanki, Y. Mishin, Atomistic modeling of capillary-driven grain boundary motion in Cu-Ta alloys, Acta Mater. 148 (2018) 311–319, doi:10.1016/j.actamat.2018.01.027.
[49] S. Srinivasan, S. Sharma, S. Turnage, B.C. Hornbuckle, C. Kale, K.A. Darling, K. Solanki, Role of tantalum concentration, processing temperature, and strain-rate on the mechanical behavior of copper-tantalum alloys, Acta Mater. 208 (2021) 116706, doi:10.1016/j.actamat.2021.116706.
[50] R.P. Carreker, W.R. Hibbard, Tensile deformation of high-purity copper as a function of temperature, strain rate, and grain size, Acta Metall. 1 (1953) 654–663, doi:10.1016/0001-6160(53)90022-4.
[51] B.L. Boyce, B.G. Clark, P. Lu, J.D. Carroll, C.R. Weinberger, The morphology of tensile failure in tantalum, Metall. Mater. Trans. A 44 (2013) 4567–4580, doi:10.1007/s11661-013-1814-8.

[52] J. Chen, S.N. Mathaudhu, N. Thadhani, A.M. Dongare, Correlations between dislocation density evolution and spall strengths of Cu/Ta multilayered systems at the atomic scales: the role of spacing of KS interfaces, Materialia 5 (2019) 100192, doi:10.1016/j.mtla.2018.100192.
[53] K.A. Darling, M.A. Tschopp, R.K. Guduru, W.H. Yin, Q. Wei, L.J. Kecskes, Microstructure and mechanical properties of bulk nanostructured Cu–Ta alloys consolidated by equal channel angular extrusion, Acta Mater. 76 (2014) 168–185, doi:10.1016/j.actamat.2014.04.074.
[54] M. Rajagopalan, K.A. Darling, C. Kale, S.A. Turnage, R.K. Koju, B.C. Hornbuckle, Y. Mishin, K.N. Solanki, Nanotechnology enabled design of a structural material with extreme strength as well as thermal and electrical properties, Mater. Today 31 (2019) 10–20, doi:10.1016/j.mattod.2019.09.024.